Applied Physics Express

LETTER

Spin transport measurements in metallic Bi/Ni nanowires

To cite this article: Masashi Tokuda *et al* 2019 *Appl. Phys. Express* **12** 053005

Applied Physics Express 12, 053005 (2019) LETTER
https://doi.org/10.7567/1882-0786/ab15ae

Spin transport measurements in metallic Bi/Ni nanowires

Masashi Tokuda[1], Natsuki Kabeya[1], Komei Iwashita[1], Hiroki Taniguchi[1], Tomonori Arakawa[1,2], Di Yue[3,4], Xinxin Gong[3,4], Xiaofeng Jin[3,4], Kensuke Kobayashi[1,2], and Yasuhiro Niimi[1,2*]

[1]Department of Physics, Graduate School of Science, Osaka University, Toyonaka, Osaka 560-0043, Japan
[2]Center for Spintronics Research Network, Osaka University, Toyonaka, Osaka 560-8531, Japan
[3]State Key Laboratory of Surface Physics and Department of Physics, Fudan University, Shanghai 200433, People's Republic of China
[4]Collaborative Innovation Center of Advanced Microstructures, Fudan University, Shanghai 200433, People's Republic of China

*E-mail: niimi@phys.sci.osaka-u.ac.jp

Received February 22, 2019; revised March 26, 2019; accepted April 3, 2019; published online April 24, 2019

We have performed spin transport measurements in metallic Bi/Ni nanowires using the spin absorption method in a lateral spin valve structure. Although Bi has a strong spin–orbit interaction, the spin Hall angle obtained for Bi/Ni nanowires is about 0.008. The magnitude and sign of the spin Hall angle are much smaller than and opposite to those of Cu–Bi alloys, where skew scattering at Bi impurities is dominant. The estimated spin diffusion length (3 nm) of Bi/Ni nanowires is shorter than that of thin Bi films, which indicates that Bi/Ni bilayers have different spin properties from Bi alone.

Bismuth is a typical semimetal and diamagnetic material. It is also known as a material with strong spin–orbit interaction because of its large atomic number. Thus, Bi-related materials have been extensively studied in the field of spintronics[1–4] where the effective generation, detection, and manipulation of spin current, flow of spin angular momentum, are central issues. For example, a large spin Hall effect, which enables us to interconvert charge and spin currents, has been realized by adding a small amount of Bi to Cu.[5,6] This large effect can also be obtained at the interface between Ag (or Cu) and Bi (or Bi_2O_3), the so-called Rashba–Edelstein effect.[7–13]

On the other hand, spin transport in Bi alone gives different results. Although Bi has a strong spin–orbit interaction, the reported spin Hall angles, the conversion ratios between charge and spin currents, are relatively small (less than a few percent).[14–17] According to recent spin Seebeck effect measurements, negligible spin-to-charge conversion has been reported in Bi films and even in Bi/Ag bilayers on $Y_3Fe_5O_{12}$ substrate.[14] The spin–orbit length, comparable to the spin diffusion length,[18] of Bi is about several tens of nanometers.[15–17,19,20]

Bi exhibits semiconducting behavior in the temperature dependence of resistivity. However, Bi/Ni bilayer thin films have a metallic transport property and even become superconductors below $\approx$4 K.[21–28] It was already known that Bi_3Ni crystals exhibit superconductivity,[29,30] but according to recent experiments,[23–28] the mechanism of superconductivity in Bi/Ni bilayers is different from that in the conventional spin-singlet Cooper pairs. Point contact measurements on Bi/Ni bilayer thin films indicate the presence of spin-triplet states.[23,28] This new type of unconventional superconductor could be useful for future superconducting spintronic devices.[31]

In this work, we aim to demonstrate spin transport properties in metallic Bi/Ni nanowires using the spin absorption method in a lateral spin valve structure.[3] The spin Hall angle of Bi/Ni obtained at 10 K is as small as 0.008, which is much smaller than that of Bi-doped Cu ($\sim$0.11) where skew scattering at Bi impurities is dominant,[5,6] but comparable to that of Bi thin films.[32,15,16] The spin diffusion length of Bi/Ni ($\approx$3 nm) at 10 K is shorter than the spin–orbit length[19,20] (30–50 nm, determined from weak antilocalization measurements) and the spin diffusion length[15–17] (10 $\sim$ 50 nm) of Bi thin films. This might be related to the fact that the Ni layer has finite magnetic moment.[24] We also investigate the superconducting state of Bi/Ni wires below 4 K.

Bi(35 nm)/Ni(2 nm) thin films were epitaxially grown on a MgO(001) substrate. For such Bi/Ni/MgO films, a high-quality heterostructure with sharp interfaces has been confirmed by reflection high-energy electron diffraction patterns and cross-sectional scanning transmission electron microscopy.[23] Using electron beam lithography on a poly-methyl–methacrylate resist and an Ar milling process, a wire with a width of 300 nm was patterned. We then prepared two ferromagnetic Permalloy ($Ni_{81}Fe_{19}$; hereafter Py) wires (30 nm thick and 100 nm wide) and a Cu wire (100 nm thick and 100 nm wide) using electron beam lithography and a subsequent lift-off process. One of the Py wires had two large pads at the ends, in order to induce a difference between the two switching fields. Careful Ar ion beam etching was carried out to obtain highly transparent interfaces between Bi/Ni and Cu as well as Py and Cu. During the nanofabrication process, the temperature was always kept below 90 °C to avoid any interdiffusion between Bi and Ni.[23]

Transport measurements were performed using a standard ac lock-in technique and a ^{4}He flow cryostat down to $T = 1.5$ K. A magnetic field was applied along the hard and easy axes of Py to measure the inverse spin Hall effect (ISHE) and nonlocal spin valve signals, respectively. In order to check reproducibility, we measured three different samples from different batches.

Figure 1 shows a scanning electron microscopy image of our spin Hall device with the metallic Bi/Ni wire. When an electric current I flows downward from the lower Py wire to the Cu stripe, spin is accumulated at the interface between Py and Cu. A spin current, which corresponds to the gradient of the spin accumulation, flows upward into the Cu channel. Since the spin diffusion length of Cu is as long as 1 μm at low temperatures,[3] the spin current does not decay much until it reaches the Bi/Ni wire. Because of the strong spin–orbit interaction of Bi/Ni, most of the spin current is absorbed perpendicularly into the Bi/Ni wire. Both the spin-up and spin-down currents flowing in opposite directions are deflected to the same direction along the Bi/Ni wire owing to the ISHE, which results in a voltage drop V_{ISHE} along the

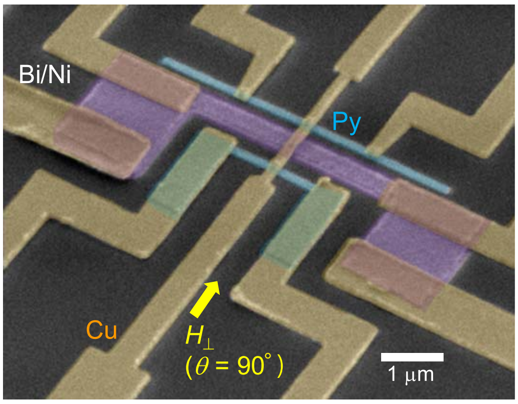

Fig. 1. (Color online) Scanning electron micrograph of a typical spin Hall device consisting of two ferromagnetic Py wires and a Bi/Ni wire bridged by a Cu stripe. The positive magnetic field direction for the inverse spin Hall effect measurement is defined as $H_\perp$ ($\theta = 90°$) by the arrow.

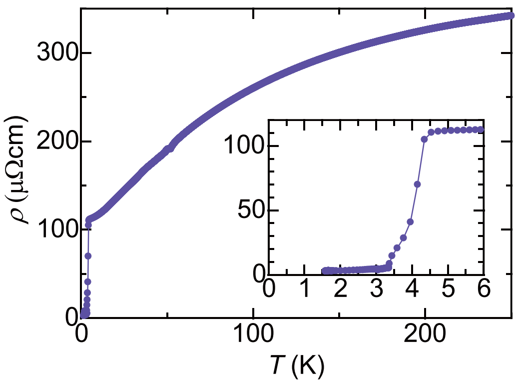

Fig. 2. (Color online) Temperature dependence of the resistivity of the Bi/Ni wire. The inset shows the closeup of the superconducting transition. The resistivity starts to decrease at 4.2 K but still has a finite value (3 $\mu\Omega$·cm) even at the lowest temperature (1.5 K).

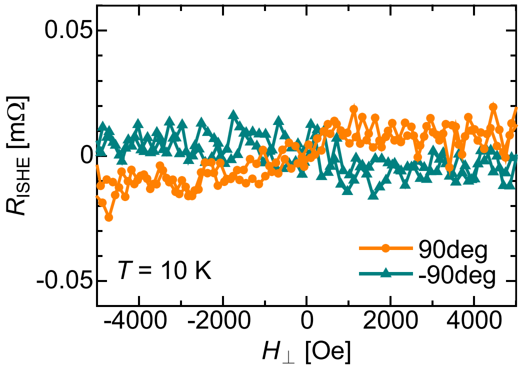

Fig. 3. (Color online) R_{ISHE} of the Bi/Ni wire measured at $T = 10$ K. The magnetic field direction is defined as indicated in Fig. 1. By inverting the field direction by 180°, the slope of R_{ISHE} between ±2000 Oe changes.

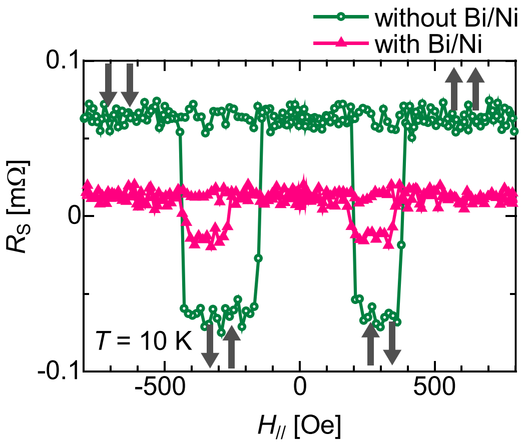

Fig. 4. (Color online) R_S at $T = 10$ K with and without the Bi/Ni wire. The arrows indicate the magnetization directions of the Py injector (left) and detector (right). By taking the ratio between the two and using Eq. (1), λ_M can be obtained.

wire. The rest of the spin current still flows in the Cu channel and is detected as a nonlocal voltage V_S at the upper Py wire.

In Fig. 2, we show the temperature dependence of the resistivity of the Bi/Ni wire in the spin Hall device. Unlike the case of pure Bi,[23,33] the resistivity of the Bi/Ni wire shows a metallic behavior and becomes a superconductor below 4.2 K. Unfortunately, however, it is not completely zero even at our lowest temperature ($T = 1.5$ K). We will return to this point below. We also fabricated Hall bar patterns and measured the Hall resistance (not shown here). The estimated electron density is 4.9×10^{22} cm^{-3}, which is much higher than that of Bi alone (3×10^{17} cm^{-3})[33] but lower than that of Ni (1.0×10^{23} cm^{-3}).[34] These results clearly show that the Bi/Ni wire is a good metal, unlike Bi alone.[23]

We next measured the ISHE in the Bi/Ni wire above the superconducting transition temperature (T_C). In Fig. 3, a typical ISHE resistance R_{ISHE} (equal to the ISHE voltage V_{ISHE} divided by the injection current I) of the Bi/Ni wire at 10 K is plotted as a function of the magnetic field ($H_\perp$) applied perpendicularly to the Py wires. The positive $H_\perp$ corresponds to $\theta = 90°$ as illustrated in Fig. 1. R_{ISHE} increases linearly with the magnetic field up to ≈2000 Oe and then flattens off at the saturation of the magnetization of the Py wire.[35] The amplitude of ISHE resistance ΔR_{ISHE} is defined as the difference between R_{ISHE} at the saturation field (above ≈2000 Oe) and R_{ISHE} at zero field, and is about 9 $\mu\Omega$. When the field direction is rotated by 180° (corresponding to $\theta = -90°$), the slope of R_{ISHE} at zero field reverses.[36] This result clearly shows that the signal originates from the ISHE in Bi/Ni.

To evaluate the spin current absorbed into the Bi/Ni wire as well as its spin diffusion length, we measured the nonlocal spin valve signal R_S (equal to the nonlocal voltage V_S between the upper Py and Cu wires, divided by the injection current I) with and without the Bi/Ni wire at 10 K; see Fig. 4. R_S has a square shape depending on the magnetization directions of the two Py wires, as indicated by the arrows. The difference in R_S between the parallel and antiparallel magnetic configurations is defined as ΔR_S. It is clear that ΔR_S is reduced by inserting the Bi/Ni wire. The ratio between $\Delta R_S^{\mathrm{with}}$ (with Bi/Ni) and $\Delta R_S^{\mathrm{without}}$ (without Bi/Ni) can be expressed as follows:[3]

$$\begin{aligned}\eta \equiv{}& \frac{\Delta R_S^{\mathrm{with}}}{\Delta R_S^{\mathrm{without}}} \\ ={}& [2R_M\{\sinh(L/\lambda_N) + 2Q_F e^{L/\lambda_N} + 2Q_F^2 e^{L/\lambda_N}\}] \\ &/[R_N\{\cosh(L/\lambda_N) - 1\} + 2R_M \sinh(L/\lambda_N) \\ &+ 2R_F\{e^{L/\lambda_N}(1 + Q_F)(1 + 2Q_M) - 1\}], \qquad (1)\end{aligned}$$

where R_N, R_F, and R_M are respectively the spin resistances of the Cu, Py, and Bi/Ni wires, $Q_F = R_F/R_N$, and $Q_M = R_M/R_N$.

The spin resistance R_X is defined as $\rho_X \lambda_X / (1 - p_X^2) A_X$, where ρ_X, λ_X, p_X, and A_X are respectively the electrical resistivity, the spin diffusion length, the spin polarization, and the effective cross-sectional area involved in the equations of the 1D spin diffusion model, and the subscript "X" represents each material (Cu, Py, or Bi/Ni). L is the distance between the two Py wires. In this study, $L = 1\ \mu$m, $R_N = 2.0\ \Omega$, $\lambda_N = 1.3\ \mu$m, and $R_F = 0.10\ \Omega$ at $T = 10$ K.[5] Thus, only the spin diffusion length λ_M of the Bi/Ni wire is left as an unknown parameter in Eq. (1). Since $\eta = 0.20$ in the present case, we obtain $\lambda_M = 2.7$ nm. This spin diffusion length is smaller than the spin–orbit length of Bi obtained with weak antilocalization[19,20] and the spin diffusion length of Bi thin films estimated from spin pumping experiments.[15–17] This result indicates that the spin transport properties of Bi/Ni are different from those of Bi alone. The difference between the two systems might originate from the fact that the Ni thin layer has finite magnetic moment.[24]

Now we discuss the spin Hall angle α_H of Bi/Ni. Based on the one-dimensional spin diffusion model, α_H can be given as

$$\alpha_H \equiv \frac{\rho_{SHE}}{\rho_{xx}} = \frac{w_M \Delta R_{ISHE}}{x \rho_{xx}} \frac{I}{\bar{I}_S}, \tag{2}$$

where w_M is the width of the Bi/Ni wire and ρ_{xx} is its resistivity. x is a shunting factor which expresses the magnitude of shunting by the Cu contact above the Bi/Ni wire. In the present case, we use $x \approx 0.18$.[37,38] $\bar{I}_S$ is the effective pure spin current injected vertically into the Bi/Ni wire:[3]

$$\begin{aligned}\frac{\bar{I}_S}{I} = {} & \frac{\lambda_M}{t_M} \frac{(1 - e^{-t_M/\lambda_M})^2}{1 - e^{-2t_M/\lambda_M}} \\ & \times [2p_F R_F \{\sinh(L/2\lambda_N) + Q_F e^{L/2\lambda_N}\}] \\ & / [R_N \{\cosh(L/\lambda_N) - 1\} + 2R_M \sinh(L/\lambda_N) \\ & + 2R_F \{e^{L/\lambda_N}(1 + Q_F)(1 + 2Q_M) - 1\}],\end{aligned} \tag{3}$$

where t_M is the thickness of the Bi/Ni wire. Using Eqs. (2) and (3), α_H of Bi/Ni is estimated to be 0.008 ± 0.002. The sign of α_H is positive, which is the same as that of Bi thin films reported in Refs. 15, 16, 32, but opposite to that of Cu–Bi alloys[5,6] and of the inverse Rashba–Edelstein effect at the interface between Cu and Bi_2O_3.[11] The magnitude of α_H is much smaller than that of Cu–Bi alloys[5,6] and at the interface between Cu and Bi_2O_3,[11] although the spin–orbit interaction of Bi should be quite strong and some theoretical calculations predict a large spin Hall conductivity.[39] This discrepancy is currently an open question.

Finally, let us discuss results on the ISHE below T_C. We had prepared another type of spin Hall device to detect quasiparticles in the superconducting Bi/Ni wire, as demonstrated in Ref. 40. Unfortunately, we could not detect a signal related to the ISHE below T_C. This is related to the fact that there is finite residual resistivity even at the lowest temperature. Retaining the high quality of the Bi/Ni wire during the nanofabrication process is necessary to observe a quasiparticle-mediated ISHE in the superconducting wire.

In summary, we have performed spin transport measurements with metallic Bi/Ni wires. The spin Hall angle of Bi/Ni at 10 K is positive and amounts to 0.008, which is similar to that of Bi thin films but is opposite to and much smaller than those of Cu–Bi alloys and the inverse Rashba–Edelstein effect at the interface between Cu and Bi_2O_3. The spin diffusion length of Bi/Ni at 10 K is as short as 3 nm, which is about one order smaller than that of Bi thin films. This might originate from the ferromagnetic Ni layer underneath the Bi layer. We have also obtained a superconducting transition in Bi/Ni wires below 4.2 K. However, there is residual resistivity even at $T = 1.5$ K and a signal related to the ISHE has not yet been obtained. This result indicates that improvement in the quality of Bi/Ni wires is needed to measure a quasiparticle-mediated ISHE in this potential spin-triplet superconductor.

Acknowledgments We thank K. Aoyama, T. Mizushima, and S. Fujimoto for fruitful discussions. We acknowledge the stimulated discussion in the meeting of the Cooperative Research Project of the RIEC, Tohoku University. This work was supported by JSPS KAKENHI (Grant Numbers JP16H05964, JP17K18756, JP26103002, and JP26220711), the National Basic Research Program of China (Grant Numbers 2015CB921402, 2011CB921802, and 2016YFA0300703), the National Natural Science Foundation of China (Grant Numbers 11374057, 11434003, and 11421404), the Mazda Foundation, Shimadzu Science Foundation, Yazaki Memorial Foundation for Science and Technology, SCAT Foundation, and the Murata Science Foundation.

ORCID iDs Yasuhiro Niimi https://orcid.org/0000-0003-1659-0634

1) J. Sinova, S. O. Valenzuela, J. Wunderlich, C. H. Back, and T. Jungwirth, Rev. Mod. Phys. **87**, 1213 (2015).
2) A. Hoffmann, IEEE Trans. Magn. **49**, 5172 (2013).
3) Y. Niimi and Y. Otani, Rep. Prog. Phys. **78**, 124501 (2015).
4) Y. Otani, M. Shiraishi, A. Oiwa, E. Saitoh, and S. Murakami, Nat. Phys. **13**, 829 (2017).
5) Y. Niimi, Y. Kawanishi, D. H. Wei, C. Deranlot, H. X. Yang, M. Chshiev, T. Valet, A. Fert, and Y. Otani, Phys. Rev. Lett. **109**, 156602 (2012).
6) C. Chen, D. Tian, H. Zhou, D. Hou, and X. Jin, Phys. Rev. Lett. **122**, 016804 (2019).
7) J. C. Rojas Sánchez, L. Vila, G. Desfonds, S. Gambarelli, J. P. Attané, J. M. De Teresa, C. Magén, and A. Fert, Nat. Commun. **4**, 2944 (2013).
8) A. Nomura, T. Tashiro, H. Nakayama, and K. Ando, Appl. Phys. Lett. **106**, 212403 (2015).
9) S. Sangiao, J. M. De Teresa, L. Morellon, I. Lucas, M. C. Martinez-Velarte, and M. Viret, Appl. Phys. Lett. **106**, 172403 (2015).
10) W. Zhang, M. B. Jungfleisch, W. Jiang, J. E. Pearson, and A. Hoffmann, J. Appl. Phys. **117**, 17C727 (2015).
11) S. Karube, K. Kondou, and Y. Otani, Appl. Phys. Express **9**, 033001 (2016).
12) M. B. Jungfleisch, Q. Zhang, W. Zhang, J. E. Pearson, R. D. Schaller, H. Wen, and A. Hoffmann, Phys. Rev. Lett. **120**, 207207 (2018).
13) C. Zhou et al., Phys. Rev. Lett. **121**, 086801 (2018).
14) D. Yue, W. Lin, J. Li, X. Jin, and C. L. Chien, Phys. Rev. Lett. **121**, 037201 (2018).
15) D. Hou et al., Appl. Phys. Lett. **101**, 042403 (2012).
16) H. Emoto, Y. Ando, E. Shikoh, Y. Fuseya, T. Shinjo, and M. Shiraishi, J. Appl. Phys. **115**, 17C507 (2014).
17) H. Emoto, Y. Ando, G. Eguchi, R. Ohshima, E. Shikoh, Y. Fuseya, T. Shinjo, and M. Shiraishi, Phys. Rev. B **93**, 174428 (2016).
18) Y. Niimi, D. H. Wei, H. Idzuchi, T. Wakamura, T. Kato, and Y. Otani, Phys. Rev. Lett. **110**, 016805 (2013).
19) F. Komori, S. Kobayashi, and W. Sasaki, J. Phys. Soc. Jpn. **52**, 368 (1983).
20) S. Sangiao, N. Marcano, J. Fan, L. Morellón, M. R. Ibarra, and J. M. De Teresa, Europhys. Lett. **95**, 37002 (2011).
21) J. S. Moodera and R. Meservey, Phys. Rev. B **42**, 179 (1990).
22) P. LeClair, J. S. Moodera, J. Philip, and D. Heiman, Phys. Rev. Lett. **94**, 037006 (2005).
23) X.-X. Gong, H.-X. Zhou, P.-C. Xu, D. Yue, K. Zhu, X.-F. Jin, H. Tian, G.-J. Zhao, and T.-Y. Chen, Chin. Phys. Lett. **32**, 067402 (2015).
24) H. Zhou, X. Gong, and X. Jin, J. Mag. Mag. Mater. **422**, 73 (2017).
25) X. Gong, M. Kargarian, A. Stern, D. Yue, H. Zhou, X. Jin, V. M. Galitski, V. M. Yakovenko, and J. Xia, Sci. Adv. **3**, e1602579 (2017).
26) J. Wang et al., Phys. Rev. B **96**, 054519 (2017).
27) P. Chauhan, F. Mahmood, D. Yue, P.-C. Xu, X. Jin, and N. P. Armitage, Phys. Rev. Lett. **122**, 017002 (2019).
28) G. J. Zhao, X. X. Gong, J. C. He, J. A. Gifford, H. X. Zhou, Y. Chen, X. F. Jin, C. L. Chien, and T. Y. Chen, arXiv:1810.10403.
29) B. Jayaram, S. N. Ekbote, and A. V. Narlikar, Phys. Rev. B **36**, 1996 (1987).
30) X. Zhu, H. Lei, C. Petrovic, and Y. Zhang, Phys. Rev. B **86**, 024527 (2012).

31) J. Linder and J. W. A. Robinson, Nat. Phys. **11**, 307 (2015).
32) J. Fan and J. Eom, Appl. Phys. Lett. **92**, 142101 (2008).
33) O. Prakash, A. Kumar, A. Thamizhavel, and S. Ramakrishnan, Science **355**, 52 (2017).
34) J. M. Lavine, Phys. Rev. **123**, 1273 (1961).
35) The saturation field of Ni alone is one order smaller than that of Py.
36) T. Kimura, Y. Otani, T. Sato, S. Takahashi, and S. Maekawa, Phys. Rev. Lett. **98**, 156601 (2007).
37) M. Morota, Y. Niimi, K. Ohnishi, D. H. Wei, T. Tanaka, H. Kontani, T. Kimura, and Y. Otani, Phys. Rev. B **83**, 174405 (2011).
38) Y. Niimi, H. Suzuki, Y. Kawanishi, Y. Omori, T. Valet, A. Fert, and Y. Otani, Phys. Rev. B **89**, 054401 (2014).
39) Y. Fuseya, M. Ogata, and H. Fukuyama, J. Phys. Soc. Jpn. **81**, 093704 (2012).
40) T. Wakamura, H. Akaike, Y. Omori, Y. Niimi, S. Takahashi, A. Fujimaki, S. Maekawa, and Y. Otani, Nat. Mater. **14**, 675 (2015).